Role of Marangoni stress during breakup of surfactant-covered liquid threads: Reduced rates of thinning and microthread cascades

Pritish M. Kamat, Brayden W. Wagoner, Sumeet S. Thete, and Osman A. Basaran
Davidson School of Chemical Engineering, Purdue University, West Lafayette, Indiana 47907, USA

(Received 12 November 2017; published 6 April 2018)

Adsorption onto and lowering of surface tension σ of fluid interfaces by surfactants is exploited in drop formation (e.g., inkjet printing) where a thinning liquid thread (radius h) connects an about-to-form drop to the liquid that remains hanging from the nozzle when the former falls from it. Surfactants can affect thread pinch-off in two ways: first, by lowering σ, they lower capillary pressure (σ/h), and second, as surfactant concentration along the interface can be nonuniform, they cause the interface to be subjected to a surface tension gradient or Marangoni stress. Recent studies show that the location where the thread breaks is devoid of surfactant, and others assert that the influence of Marangoni stress on pinch-off is negligible. We demonstrate by simulations and experiments that surfactants play a major role in drop formation and that Marangoni stresses acting near but not at the pinch point give rise to reduced rates of thread thinning and formation of multiple microthreads that distinguish pinch-off of surfactant-covered threads from surfactant-free ones. Thinning at finite Reynolds and Peclet numbers, Re and Pe, is shown to exhibit intermediate scaling regimes that have heretofore only been observed during pinch-off of threads undergoing creeping flow (Re = 0) while convection of surfactant is weak compared to its diffusion (Pe < 1).

DOI: 10.1103/PhysRevFluids.3.043602

I. INTRODUCTION

In drop formation, liquid flows out of a nozzle and feeds a growing pendant drop that hangs from it [Fig. 1(a)]. The growing pendant drop consists of an about-to-form primary drop, a thinning liquid thread, and a hemispherical mass of liquid attached to the nozzle [Fig. 1(b)]. Thinning of the thread and its eventual pinch-off, both salient features of drop formation processes involving dripping and jetting [1,2], are driven by capillary pressure (≈surface tension/thread radius). The thread's shape near the space-time singularity where the interface will pinch off—and result in a primary drop falling from the nozzle—is self-similar and its evolution in time is governed by scaling laws [3,4]. For Newtonian fluids, in the absence of external noise [5], the interface shape near the pinch point consists of a main thread that is connected to the primary drop by a much thinner but shorter microthread [Fig. 1(c)]. Once the thread breaks and the primary drop detaches, the thread may also pinch off at its top and undergo multiple breakups to give birth to satellite droplets [6]. Controlled drop formation—production of identical primary drops in succession while minimizing satellites—is used in myriad applications [1,4,7,8]. Because of the central role it plays in drop formation, studying the breakup of liquid threads and jets has been a problem at the forefront of science for nearly two centuries [2,4].

Surfactants are used widely in drop formation applications. Figure 1(d) depicts experiments where a surfactant, sodium dodecyl sulfate (SDS), is present at the air-liquid interface and shows that the dynamics of drop formation is altered radically compared to situations when surfactants are absent: a cascade of microthreads, each thinner than the one preceding it and which had heretofore only been seen in simulations [9], arises between the main thread and the primary drop. The startling difference

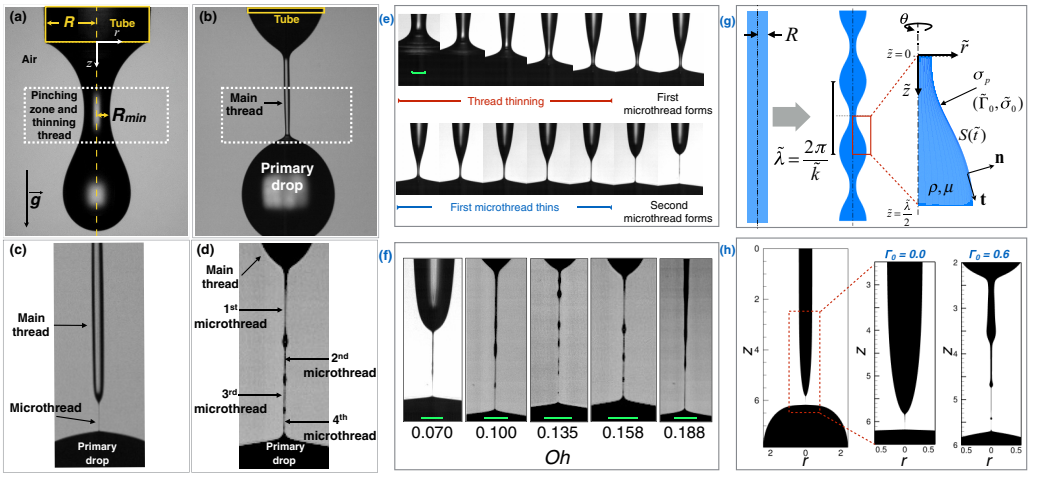

FIG. 1. Pinch-off and microthread cascades. (a)–(d) Drop formation from a tube: (a) A glycerol-water (GW) drop showing the pinching zone and a thread of minimum radius $R_{\min}$ and (b) the same drop later in time showing the about-to-form primary drop and main thread. Zoomed-in views of the pinching zone depicting the main thread and either (c) a single microthread when the surfactant-free drop of (a), (b) is about to pinch off or (d) a cascade of four microthreads when a surfactant-laden GW drop is about to break. (a)–(c), Oh $= 0.2$, and (d) Oh $= 0.158$ and the concentration of surfactant (SDS) is 2 cmc (critical micelle concentration). (e) Time evolution of the pinching zone for a GW drop of Oh $= 0.07$ loaded with SDS (concentration $= 1.5$ cmc). (f) Breakup shapes of GW drops loaded with SDS (concentration $= 1.5$ cmc) as a function of Oh. (g) Definition sketch for simulations. (h) Jet profiles at pinch-off from simulations when Oh $= 0.12$ and $k = 0.4$. A surfactant-free jet: profile over half a wavelength (left) and zoomed-in view of pinching zone (middle). A surfactant-covered jet of $\beta = 0.4$: zoomed-in view of pinching zone showing four microthreads (right). (Green scale bars in (e) and (f) equal 76.5 μm.)

in interface shapes of surfactant-free and surfactant-laden threads is surprising as theoretical [10–12] studies have shown that strong flows evacuating the pinching neck between the main thread and primary drop convect surfactant away from it and cause it to be devoid of surfactant at pinch-off. Furthermore, it is well known that surfactants slow the rate of thread thinning, increase drop lengths at breakup, and alter sizes of primary drops [9,10,12–16]. How do surfactants affect breakup so drastically in absentia?

Surfactants can affect surface-tension-driven flows such as thread breakup in two ways. First, because they lower surface tension when they adsorb onto air-water interfaces, surfactants reduce capillary pressure compared to situations when the interface is surfactant free [17]. Second, because their concentration along the interface can be nonuniform, they can cause the interface to be subjected to a surface-tension-gradient-induced or Marangoni stress [18], which plays a central role in well-known phenomena such as tears of wine and Benard cells in thin films [19]. Despite two decades of research on breakup of surfactant-laden threads, there is disagreement as to which of the two mechanisms is responsible for the observed differences between pinch-off of surfactant-free and surfactant-covered threads. Thus, while several studies attribute the observed effects to the action of Marangoni stresses [9,10,12,13], more recent works [14–16] attribute them to lowering of surface tension, and hence capillary pressure. In this paper, we use numerical simulations supported by experiments to demonstrate how surfactants induce formation of microthread cascades and reduce rates of thread thinning. Because it is challenging to separate competing effects of surface tension lowering and surface tension gradients in experiments, we perform simulations in which Marangoni stresses are turned off—a feat that would not be possible to accomplish experimentally—to demonstrate conclusively that Marangoni stress is the dominant mechanism by which surfactants affect pinch-off.

TABLE I. Key experimental parameters: combinations of tube radii R and glycerol concentrations in water by weight percent (Gly wt%) used to achieve the range of Ohnesorge numbers (Oh) used in the experiments.

R (mm)	Gly wt%	Oh
1.57	70	0.07
2.4	77.5	0.1
1.57	77.5	0.135
1.16	77.5	0.158
0.82	77.5	0.188

The paper is organized as follows. As the formation of microthread cascades during the pinch-off of surfactant-covered threads had heretofore only been seen in simulations [9], we first carried out experiments on dripping of surfactant-laden liquids from a tube, which are described in Sec. II, to demonstrate their occurrence in the laboratory. The next section, Sec. III, provides the mathematical formulation of the problem of thinning and breakup of surfactant-covered threads and summarizes the numerical method used to simulate thread thinning and pinch-off. The results of the simulations are then presented in Sec. IV. Section V concludes the article with an extensive discussion on how the theoretical and simulation approaches used in this paper can be applied to analyze a number of other physical problems in fluid mechanics as well as in other fields of science in which surfactant-covered interfaces are present and Marangoni stress may play a dominant role.

II. EXPERIMENTS

In the experiments, aqueous solutions of different concentrations of glycerol in water were prepared. These solutions had density, viscosity, and surface tension of ρ, μ, and σ_p. In some experiments, SDS was added to these solutions at concentrations exceeding the cmc. At the concentrations used, the density and viscosity of the solutions were unchanged by addition of surfactant. The surfactant-free and surfactant-laden solutions were then dripped at low flow rate Q from a tube of radius R in air. In addition to surfactant concentration expressed as a multiple of the cmc, the dynamics of drop formation is governed by Weber number $\mathrm{We} \equiv \rho(Q/\pi R^2)^2 R/\sigma_p$ (here $\mathrm{We} \ll 1$), gravitational Bond number $G \equiv \rho g R^2/\sigma_p \approx O(0.1)$ (G varied slightly in the experiments given the slight variation of ρ and σ_p with glycerol concentration), and Ohnesorge number $\mathrm{Oh} \equiv \mu/\sqrt{\rho R \sigma_p}$. In the experiments, a range of Oh values were obtained by varying the nozzle radius between 0.82 and 2.4 mm and the concentration of glycerol between 70 and 77.5 wt % in water (see Table I).

Figure 1(e) shows a zoomed-in view of the pinching zone when a surfactant-laden drop of a GW solution of $\mathrm{Oh} = 0.07$ is forming from a nozzle. This figure depicts the evolution in time of the interface shapes as the main thread thins, a first microthread forms and thins, and a second microthread forms just prior to rupture. Figure 1(f) shows the variation of microthread cascades with Oh when surfactant-laden drops are formed from a nozzle. Plainly, microthread cascades composed of two to as many as seven microthreads can arise during the dripping of surfactant-laden liquids.

III. MATHEMATICAL FORMULATION AND NUMERICAL METHOD

A. Mathematical formulation

To gain insights into the formation of microthread cascades, we turn to numerical simulations and adopt the simplest configuration possible: an infinite liquid column or jet of unperturbed radius R surrounded by a dynamically passive gas (air) that when subjected to axisymmetric shape perturbations of infinitesimal amplitude $\tilde{\delta}$ ($\tilde{\delta}/R \ll 1$), having axial wavelength $\tilde{\lambda}$ (or wave number $\tilde{k} = 2\pi/\tilde{\lambda}$), undergoes capillary or Rayleigh-Plateau instability if $\tilde{\lambda} > 2\pi R$ [20,21] [Fig. 1(g)]. As

in the experiments, the liquid is incompressible, isothermal, and Newtonian. In the simulations, the jet's free surface or the interface $S(\tilde{t})$, where $\tilde{t}$ is time, is taken to be initially coated uniformly with a monolayer of an insoluble surfactant at concentration $\tilde{\Gamma}_0$. Surface tension is taken to vary with surfactant concentration $\tilde{\Gamma}$ according to the Szyszkowski equation [19]:

$$\tilde{\sigma} = \sigma_p + \Gamma_m R_g T \ln(1 - \tilde{\Gamma}/\Gamma_m), \tag{1}$$

where Γ_m is the maximum packing value of $\tilde{\Gamma}$, R_g is the gas constant, and T is the temperature. The dynamics of surfactant-laden jets is governed by the following dimensionless groups: Ohnesorge number $\mathrm{Oh} \equiv \mu/(\rho R \sigma_p)^{1/2}$, strength of surfactant parameter $\beta \equiv \Gamma_m R_g T/\sigma_p$, surface Péclet number $\mathrm{Pe} \equiv (1/D_s)\sqrt{\sigma_p R/\rho}$ [relative importance of convection of surfactant to its diffusion on $S(\tilde{t})$], where D_s is the surface diffusivity of the surfactant, dimensionless wavelength $\lambda \equiv \tilde{\lambda}/R$ or wave number $k \equiv \tilde{k}R$, dimensionless amplitude of the initial perturbation $\delta \equiv \tilde{\delta}/R$, and dimensionless initial surfactant concentration $\Gamma_0 \equiv \tilde{\Gamma}_0/\Gamma_m$. Here, we use $\mathrm{Pe} = 1\times10^3$ and $\beta = 0.2$–0.4 as $\mathrm{Pe} \gg 1$ in practice and the range of β values is typical for strong surfactants [9,22].

Whereas the surfactant in the experiments is soluble, that in the simulations is insoluble and hence confined to the gas-liquid interface. However, the solubility of SDS in GW mixtures does not affect the surface tension or its gradient along the interface in studying pinch-off as the surface-adsorption dynamics of SDS is at least two orders of magnitude slower than the flow dynamics [14], which takes place over the inertial-capillary time scale $t_c = (\rho R^3/\sigma_p)^{1/2}$ when $\mathrm{Oh} \ll 1$, the viscocapillary time scale $t_v = \mu R/\sigma_p = \mathrm{Oh} t_c$ when $\mathrm{Oh} \gg 1$, and the viscous time scale $t_\mu = \mu^3/\rho\sigma_p^2 = \mathrm{Oh}^3 t_c$ when $\mathrm{Oh} \sim 1$.

The dynamics of jet breakup is analyzed by solving the transient free boundary problem consisting of the Navier-Stokes and continuity equations for fluid velocity $\tilde{\boldsymbol{v}}$ and pressure $\tilde{p}$ in cylindrical coordinates $(\tilde{r},\tilde{z})$, where $\tilde{r}$ and $\tilde{z}$ are the radial and axial coordinates, over the domain of axial extent equal to one-half of the wavelength of the imposed perturbation simultaneously with the surface convection-diffusion equation for surfactant concentration $\tilde{\Gamma}$ along the liquid-gas interface [22]. These equations are solved subject to the traction and kinematic boundary conditions at the liquid-gas interface and symmetry boundary conditions at both $\tilde{z} = 0$ and $\tilde{z} = \tilde{\lambda}/2$. The initial condition is such that the thinning of the jet is initiated by subjecting the surface of a jet that is uniformly coated with a surfactant to a shape perturbation as described in the opening paragraph of this section. Hereafter, the results are presented in terms of dimensionless variables such that the dimensionless velocity, pressure, surfactant concentration, surface tension, radial and axial coordinates, and time are given by $\boldsymbol{v} = \tilde{\boldsymbol{v}}/(R/t_c)$, $p = \tilde{p}/(\sigma_p/R)$, $\Gamma = \tilde{\Gamma}/\Gamma_m$, $\sigma = \tilde{\sigma}/\sigma_p$, $r = \tilde{r}/R$, $z = \tilde{z}/R$, and $t = \tilde{t}/t_c$.

B. Numerical method

The aforementioned transient system of governing equations is solved numerically by means of a fully implicit, arbitrary Lagrangian-Eulerian (ALE) method-of-lines algorithm in which the Galerkin finite element method (GFEM) is used for spatial discretization [23,24] and an adaptive, implicit finite difference method is employed for time integration [25,26]. In order to capture the large deformations that the jet's free surface and hence the domain enclosed beneath the jet's free surface can undergo, the elliptic mesh generation method developed by Christodoulou and Scriven [27] for analyzing thin-film coating flows, and which was later extended to simulate free-surface flows of Newtonian and complex fluids undergoing breakup or coalescence [6,22,28–32], was used to discretize the spatial domain $\Omega(t)$ and determine the radial and axial coordinates of each grid point in the moving, adaptive mesh simultaneously with the velocity and pressure unknowns in the jet as well as the free-surface profile and surfactant concentration along the interface. Here, the velocity and pressure unknowns were solved in the mixed interpolation sense using biquadratic basis functions to represent the velocity unknowns and bilinear basis functions to represent the pressure unknowns [33,34]. The locations of the mesh coordinates were also represented using biquadratic basis functions. The surfactant concentration at the interface was determined using a set of one-dimensional quadratic basis functions [35].

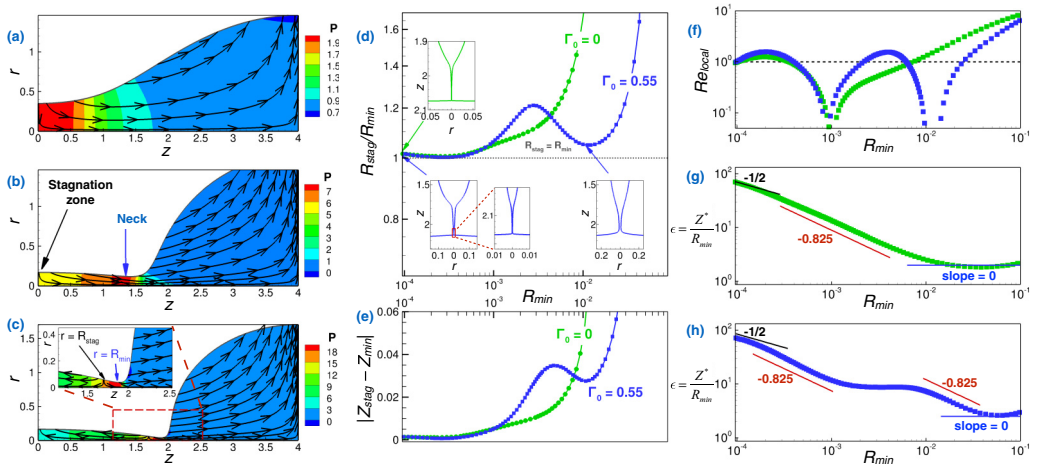

FIG. 2. Stagnation zone recoil and microthread cascade formation. Simulation results shown are for Oh = 0.07 and $k = \pi/4$. For the surfactant-covered jet, $\Gamma_0 = 0.55$ and $\beta = 0.3$. (a)–(c) Jet profiles, streamlines, and (colored) pressure contours. Profiles of surfactant-covered jet when (a) $R_{\min} = 3.5\times10^{-1}$ and the neck is located at $z = 0$, (b) $R_{\min} = 1.2\times10^{-1}$ and the neck has moved away from $z = 0$, and (c) $R_{\min} = 4.1\times10^{-2}$ and the stagnation zone has approached the neck (inset: zoomed-in view of stagnation zone and neck). (d) Variation of $R_{\text{stag}}/R_{\min}$ with $R_{\min}$ for the surfactant-free (green) and surfactant-covered (blue) jet. Insets: Zoomed-in views of the neck regions to highlight microthread formation. (e), (f) Variation with $R_{\min}$ of (e) $|Z_{\text{stag}} - Z_{\min}|$ and (f) Re_{local} for the surfactant-free (green) and surfactant-covered (blue) jet. (g), (h) Variation of thread aspect ratio $\epsilon = Z^*/R_{\min}$ with $R_{\min}$ for (g) surfactant-free and (h) surfactant-covered jet.

The numerical scheme reduces the problem to a system of nonlinear algebraic equations that can be solved iteratively via a multidimensional Newton method. The resulting system of linear equations is then solved with a frontal algorithm which takes advantage of the sparsity of the Jacobian matrix that arises in Newton's method. This frontal algorithm was inspired by the frontal method introduced by Hood [36]. For a more complete description of the numerical method that has been employed, the reader is referred to Refs. [6,22].

IV. RESULTS AND DISCUSSION

Figures 2(a)–2(c) show at three instants profiles of a thinning jet, and the instantaneous streamlines and pressure contours within it. On account of the initial conditions, at $t = 0$ the jet's neck and bulge lie at the two symmetry planes $z = 0$ and $z = \lambda/2$. Thus, given the initial perturbation of the jet's surface, capillary pressure p_c is a maximum at the neck and a minimum at the bulge. Figure 2(a) shows that at early times, the neck, with radius and axial location $R_{\min}$ and $Z_{\min}$, remains at $z = 0$, and that the radius of the neck falls as that of the bulge grows as fluid is driven from the neck to the bulge because of the capillary pressure gradient [21]. For all times, because of the axially periodic nature of the problem, the axial velocity equals zero at both $z = 0$ and $z = \lambda/2$ and both locations are therefore stagnation zones. Henceforth, we denote by $(R_{\text{stag}}, Z_{\text{stag}})$ the location of the point along the free surface where the stagnation point that is closest to the neck is located. At early times, both the minimum radius and the aforementioned stagnation point lie at the neck.

As fluid evacuates the neck, it accelerates in the direction of motion, before decelerating again in the bulge. When Oh $\ll 1$, viscous resistance is too weak to oppose the fluid's acceleration. Therefore, the jet tends to thin fastest where fluid acceleration is highest, thereby causing the neck to migrate from its initial location toward the bulge. This inertial movement of the neck is well known in low-Oh systems [37–39] and is what causes satellite droplets to form in dripping and jetting [40]. Figure 2(b) shows the jet at the instant when the neck has already moved away from $z = 0$ and is

now located at $z = Z_{\min} = 1.4$. Since the capillary pressure is nearly inversely proportional to the thread radius, the pressure maximum always lies at the neck. As a consequence of neck migration, a pressure gradient arises between where the neck is currently located and the symmetry plane $z = 0$, and which now opposes fluid flowing from the vicinity of the symmetry plane toward the neck. As the neck continues to thin and the magnitude of the capillary force opposing the inertia of the fluid grows, the flow on the thread side of the neck decelerates and ultimately reverses direction, giving birth to a stagnation zone [Fig. 2(c)] at a location $z = Z_{\text{stag}}$, where $0 \ll Z_{\text{stag}} < Z_{\min}$. The newly formed stagnation zone continues to travel toward the neck as the thinning continues. Governed by the inertia of the fluid, the dynamics that has just been described constitutes the requisite first step in the formation of microthread cascades.

The relative motion between the stagnation zone and the neck can be appreciated by plotting the variation with the minimum jet radius $R_{\min}$ of (a) the ratio of jet radius at the stagnation zone and that at the neck, $R_{\text{stag}}/R_{\min}$, and (b) the absolute value of the axial location of the stagnation zone relative to that of the neck, $|Z_{\text{stag}} - Z_{\min}|$, as in Figs. 2(d) and 2(e). As the stagnation zone begins its journey toward the neck, $R_{\text{stag}}/R_{\min} \to 1$ and $|Z_{\text{stag}} - Z_{\min}| \to 0$. In the surfactant-free case, the stagnation zone approaches the neck monotonically such that it moves faster in the axial direction than the neck until pinch-off. By contrast, Figs. 2(d) and 2(e) show that when surfactants are present, this motion is hindered: relative to the neck, the stagnation zone appears to recoil backward before resuming its motion toward the neck.

During the period when the neck migrates from its initial location ($z = 0$), the dynamics is governed by an inertial-capillary balance and the thread appears conical [37,38] as it joins the bulge. In the absence of viscosity, this state of affairs persists until pinch-off. For finite viscosity, however, the universal solution of Eggers [3] dictates that the shape of the thread joining the bulge should be slender and nearly cylindrical as opposed to conical. Indeed, it is known and shown by a shape inset in Fig. 2(d) that in the absence of surfactants, the thread possesses a conical structure but terminates in a nearly cylindrical microthread to satisfy Eggers's solution. Recent work [41] (see also Ref. [42]) indicates that this transition to Eggers's solution occurs as the stagnation zone approaches the neck and causes the dynamics to transition momentarily from inertial-capillary flow to viscous flow, thereby heralding the birth of a single microthread. This transition can be observed by plotting the variation with $R_{\min}$ of the local Reynolds number $\text{Re}_{\text{local}} = Z^* V^*/\text{Oh}$ [41], a measure of the relative importance of inertial to viscous forces near the neck, where Z^* and V^* are the axial length and velocity scales [Z^* is evaluated using the value of the in-plane or axial curvature of $S(t)$ at the neck which scales as $R_{\min}/(Z^*)^2$ and V^* is evaluated on $S(t)$ where the thread radius equals $1.05 R_{\min}$]. In the surfactant-free case, Re_{local} is seen to drop from a value that is initially much larger than unity as the stagnation zone migrates from $z = 0$ to a value that is much smaller than unity as the stagnation zone approaches the neck [Fig. 2(f)]. In the viscous regime, the slenderness of the just-formed microthread grows rapidly as the jet continues to thin [Fig. 2(g)]. As time advances, fluid velocity near the neck starts to rise and Re_{local} [Fig. 2(f)] becomes order unity as the dynamics transitions to an inertial-viscous regime and the jet tends toward pinch-off.

For surfactant-covered jets, the early time response is similar to that for surfactant-free jets. Re_{local} again falls from a large to a small value as the stagnation zone approaches the neck as a viscouslike (see below) regime is attained [Fig. 2(f)]. The jet profile [Fig. 2(d)] shows that a single microthread has already formed. Shortly thereafter, however, the stagnation zone recoils, dynamics is thrown off the viscouslike regime, and Re_{local} starts to increase. The stagnation zone then starts to approach the neck once again, the flow slows, and a new microthread begins to form. The second microthread too elongates, the flow speeds up, and $\text{Re}_{\text{local}} \to O(1)$ as the jet tends toward breakup. In the two viscouslike and the final regimes, the microthreads undergo rapid stretching [Fig. 2(h)] similar to surfactant-free jets [Fig. 2(g)], a point returned to below. Computations reveal that when surfactants are present, the number of times the stagnation zone approaches the neck equals the number of microthreads formed. Clearly, the key to understanding repeated microthread formation lies in investigating how surfactant transport along the interface interacts with fluid flow within the jet to cause stagnation zone recoil.

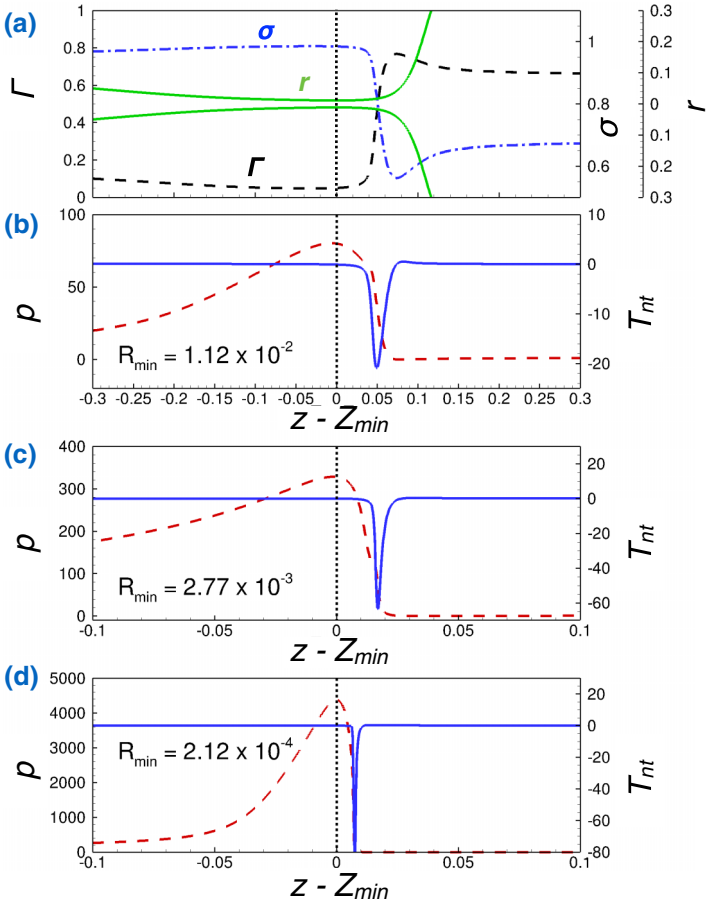

FIG. 3. Competition between pressure and Marangoni stress. (a) Jet profile, surfactant concentration, and surface tension as a function of $z - Z_{\min}$ when $R_{\min} = 1.12\times10^{-2}$. Pressure p (dashed red curve) and Marangoni stress T_{nt} (solid blue curve) as a function of $z - Z_{\min}$ at three instants: (b) just before stagnation zone recoil, (c) just after recoil, and (d) during late stages. The vertical dotted black line indicates the instantaneous location of the neck. Here, the dimensionless groups are the same as those in Fig. 2.

As the thread thins, the steep pressure drop from the neck to the bulge and the concomitant convection of surfactant from the thread to the bulge leads to depletion of surfactant in the thread and accumulation of surfactant in the bulge and, therefore, lower surface tension in the bulge compared to the relatively surfactant-lean thread. Figure 3(a) shows the interface shape and surfactant concentration and surface tension profiles just before stagnation zone recoil takes place. The resulting surface tension gradient gives rise to a large Marangoni stress, $T_{nt} = \boldsymbol{t} \cdot \nabla_s \sigma$, where $\boldsymbol{t}$ is the unit tangent to $S(t)$ (directed toward the bulge) and ∇_s is the surface gradient operator, just downstream of the neck [Fig. 3(b)]. Thus, the negative spike in T_{nt} represents a Marangoni stress pointing away from the bulge toward the main thread, directly opposing the driving pressure drop. Figure 3(c) shows the pressure and Marangoni stress profiles in the vicinity of the neck ($z = Z_{\min}$) just after recoil. It is noteworthy that Marangoni stress always runs counter to the driving pressure drop, and that the balance takes place away from the neck, i.e., nonlocally. During the early stages of thinning and up to the point when the stagnation zone is about to recoil [Figs. 3(a) and 3(b)], Marangoni stress rises to a value that is comparable in magnitude to pressure. Beyond that point in time, however, the maximum value of $|T_{nt}|$ no longer increases [Figs. 3(c) and 3(d)] as it is limited by the amount of surfactant

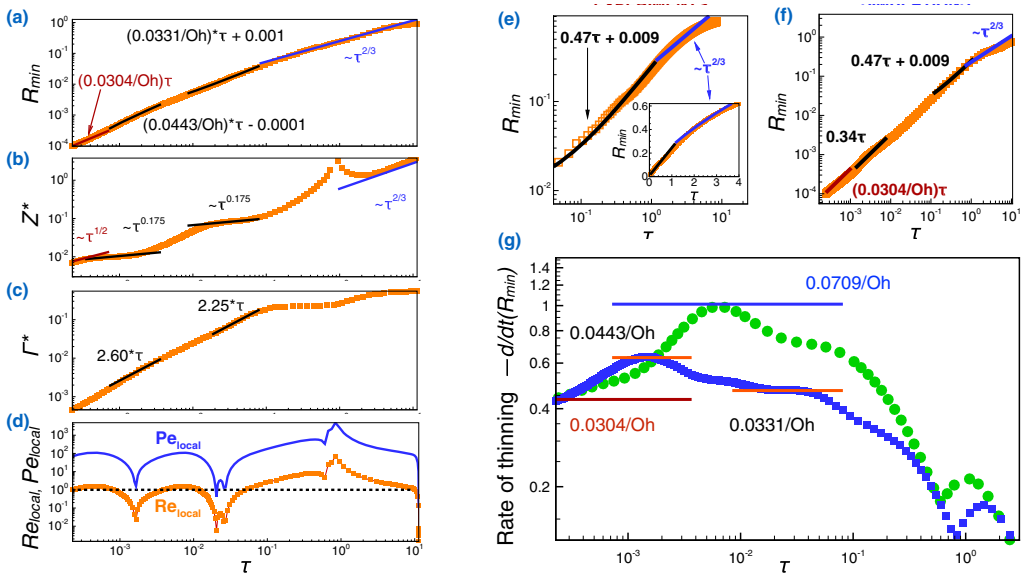

FIG. 4. Scaling results, experimental confirmation, and rate of thinning. (a)–(d) Scaling results for the surfactant-covered jet of Fig. 2: variation with τ of (a) minimum neck radius $R_{\min}$, (b) axial length scale Z^*, (c) surfactant concentration at the neck Γ^*, and (d) $\mathrm{Re}_{\mathrm{local}}$ and $\mathrm{Pe}_{\mathrm{local}}$. Experimental confirmation of scaling results: (e) $R_{\min}$ versus τ obtained from dripping experiments performed with a fluid of $\mathrm{Oh} = 0.07$ loaded with SDS at 2 cmc showing transition from I to VWM scaling (inset: same data plotted on a linear scale to highlight the large duration of the I regime.) and (f) $R_{\min}$ versus τ obtained from simulations of a breaking jet of $\mathrm{Oh} = 0.07$, $k = \pi/4$, $\Gamma_0 = 0.6$, and $\beta = 0.4$. (g) Rate of thinning $(-\frac{d}{dt}R_{\min})$ as a function of τ for the jet from Fig. 2 (blue curve) and for the same jet without surfactants (green curve).

that is available. On the other hand, the maximum value of pressure grows by several orders of magnitude during this period [Figs. 3(c) and 3(d)]. Therefore, prior to recoil, fluid being evacuated from the stagnation zone suddenly encounters Marangoni opposition before entering the bulge, the negative reaction of which causes the source of the flow—the stagnation zone—to recoil. Is it possible to validate this hypothesis that such a nonlocal Marangoni stress-capillary pressure competition is responsible for stagnation zone recoil and, therefore, occurrence of multiple microthreads?

To determine the dominant balance of forces, the variation with time of the minimum neck radius $R_{\min}$, the axial length scale Z^*, the axial velocity scale V^*, and the local surfactant concentration at the neck, Γ^* [43], along with the local Reynolds number $\mathrm{Re}_{\mathrm{local}}$ and the local Péclet number $\mathrm{Pe}_{\mathrm{local}} = Z^*V^*\mathrm{Pe}$, a measure of the effectiveness of convection in the vicinity of the neck, are monitored. Figures 4(a)–4(d) show the evolution of these scales, obtained from the simulations of the same jet as in Figs. 2 and 3, with the dimensionless time from breakup, $\tau = (t_{\mathrm{break}} - t)/t_c$, on log-log plots.

Since Oh in this case is less than 1 ($\mathrm{Oh} = 0.07$), and the early stages of thinning, when the neck migrates from $z = 0$, entail a competition between fluid inertia and the opposing pressure gradient, the dynamics are expected to reflect the underlying inertial-capillary balance. Studies of thinning of surfactant-free threads under such conditions have shown that the dynamics follow the inertial scaling law (or I scaling) [37,38], where $R_{\min} \sim \tau^{2/3}$ and $Z^* \sim \tau^{2/3}$. Reassuringly, simulation results of Figs. 4(a) and 4(b) show that the computed values of both $R_{\min}$ and Z^* vary as $\tau^{2/3}$ as expected and Fig. 4(c) shows that Γ^*, and hence surface tension, varies only slightly with τ. Moreover, Fig. 4(d) shows that $\mathrm{Re}_{\mathrm{local}}, \mathrm{Pe}_{\mathrm{local}} > 1$ at early times, as is appropriate since inertia dominates viscous force. However, once a stagnation zone forms at $z \neq 0$ and travels toward the neck, the flow in the vicinity of the neck slows and $\mathrm{Re}_{\mathrm{local}} \ll 1$. For surfactant-free threads, it has been shown [41] that this happens

once and gives rise to a viscocapillary balance that follows the viscous scaling law (or V scaling) [44], where $R_{\min} \sim \tau$ and $Z^* \sim \tau^{0.175}$. When surfactants are present, the stagnation zone approaches the neck several times between recoils, causing $\mathrm{Re}_{\mathrm{local}}$ to become much smaller than 1 during each approach. For the surfactant-laden thread of Figs. 2–4, this occurs twice.

Xu *et al.* [43] analyzed theoretically thinning of surfactant-covered jets in the absence of inertia ($\mathrm{Re} = 0$) for small Pe. These authors thereby demonstrated that two different scaling regimes are possible, each of which involves either a weak or a strong coupling between Marangoni force on the one hand and viscous and capillary forces on the other hand. In the weak type of interaction, i.e., viscous-weak Marangoni or VWM scaling, they showed that $R_{\min} \sim \tau$, $Z^* \sim \tau^{0.175}$, and $\Gamma^* \sim \tau$. Figures 4(a)–4(d) show that the simulation results predict that when both $\mathrm{Re}_{\mathrm{local}}$ and $\mathrm{Pe}_{\mathrm{local}}$ attain values much less than 1, $R_{\min}$, Z^*, and surfactant concentration at the neck all vary with τ in accordance with VWM scaling. Hence, the observed response when $\mathrm{Re}_{\mathrm{local}}, \mathrm{Pe}_{\mathrm{local}} \ll 1$ validates our hypothesis of viscocapillary interactions being responsible for stagnation zone recoil while demonstrating that the nature of this interaction is VWM scaling where a non-negligible but weak Marangoni stress acts in the presence of dominant (normal) viscous stress and capillary pressure. During this period, viscous and capillary forces scale as $\tau^{-1.175}$, whereas Marangoni stress scales as $\tau^{-0.175}$. In discussing Fig. 3, it was reported that in the late stages of breakup as $R_{\min} \to 0$, the capillary pressure at the neck grows without bound as $1/R_{\min}$ and dwarfs the opposing Marangoni stress whose magnitude saturates as surfactant has virtually completely convected out of the neck. Therefore, as shown in Fig. 4, after proceeding through the multiple VWM regimes, the dynamics transitions into Eggers's inertial-viscous (IV) scaling regime [3], where $R_{\min} = (0.0304/\mathrm{Oh})\tau$ and $Z^* \sim \tau^{1/2}$, as has already been shown by others [10–12,22]. Thus, surfactant-laden jets, after thinning in an early I-stage scaling regime, exhibit multiple transitory VWM regimes before settling into a final IV regime as they tend to pinch-off. Moreover, each VWM regime is associated with the stagnation zone approaching the neck and, therefore, the formation of one more microthread. Microthread aspect ratios $\epsilon = Z^*/R_{\min}$ of Figs. 2(g) and 2(h) can also finally be rationalized given the scalings for Z^* and $R_{\min}$ reported in this and the previous paragraph.

In Figs. 4(e) and 4(f), a comparison is provided between experimental measurement and computational prediction of the variation of $R_{\min}$ with τ for a system with properties that are slightly different than those of Figs. 4(a)–4(d) (also, see the discussion below of Fig. 6 and the Appendix). In each case, after the decay of initial transients, the dynamics starts in an initial I regime and then transitions to a VWM regime. In the experiments, it is not possible to image the drops beyond this point as $R_{\min}$ becomes of the order of microns. However, the simulations are readily continued beyond this point and reveal the occurrence of a second VWM regime which eventually gives way to a final IV regime as $R_{\min} \to 0$.

Equally noteworthy are the rates at which the necks of threads thin. Simulation results of Fig. 4(g) show that surfactant-free threads exhibit much higher thinning rates than surfactant-covered ones. During thinning, a surfactant-free thread attains a thinning rate as high as $0.0709/\mathrm{Oh}$ while in the intermediate viscous (V) regime [44] before eventually converging onto the single value of $0.0304/\mathrm{Oh}$ appropriate for the final Eggers regime [3] as the thread tends to pinch off. By contrast, the surfactant-covered thread exhibits two periods when the thread thins at a constant rate and during both of which the dynamics lies in the VWM regime.

To prove the hypothesis that Marangoni stress is primarily responsible for both reduced thinning rates and occurrence of multiple microthreads, simulations are carried out in which Marangoni stress or the surface tension gradient is turned off, $\nabla_s \sigma = 0$, while capillary pressure, which depends on surface tension, is left turned on. Figure 5 shows profiles of microthreads at breakup and thinning rates for a surfactant-covered thread, a surfactant-free thread, and a surfactant-covered thread with Marangoni stress turned off. Plainly, the Marangoni-free case resembles the surfactant-free case in all respects, including a single, short microthread and high thinning rates. On the other hand, three microthreads and lower thinning rates are produced in the presence of Marangoni stress, thus settling the long-standing debate that Marangoni stress is *primarily* responsible for both reduced

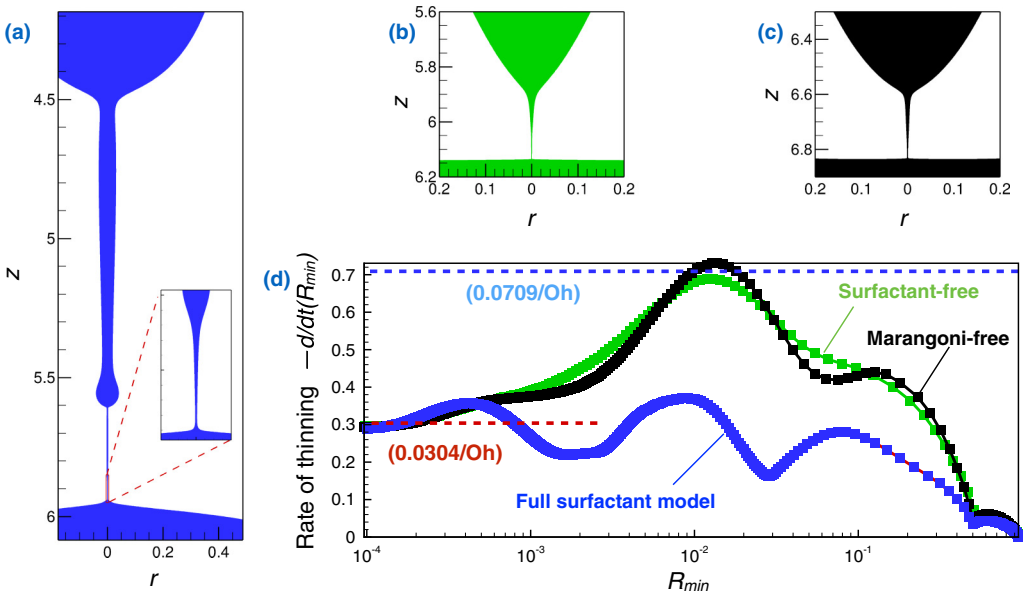

FIG. 5. Jets with and without Marangoni stress. Zoomed-in views of microthreads of (a) surfactant-covered jets, (b) surfactant-free jets, and (c) surfactant-covered jets but with Marangoni stress turned off. Because vertical distances are to scale, the drastic difference in microthread lengths is noteworthy. (d) Thinning rate versus $R_{\min}$ for surfactant-covered jet (full surfactant model), surfactant-free jet (surfactant-free), and surfactant-covered jet but with Marangoni stress turned off (Marangoni-free). Here, Oh $= 0.10$ and $k = 0.4$. For the cases with surfactants, $\Gamma_0 = 0.55$ and $\beta = 0.3$.

rates of thinning and formation of microthread cascades during capillary thinning and breakup of surfactant-covered threads.

Furthermore, Roché *et al.* [14], who performed careful experiments on SDS-water-glycerol systems similar to those carried out here, assert that local surface tension at the neck alone determines the thinning rate. In order to critically evaluate their claim, we provide a side-by-side comparison in Fig. 6 of the scaling results for $R_{\min}$ that they have obtained experimentally [in Fig. 6(a), where we have replotted their Fig. 4(b)] and the scaling predictions from our simulations [Fig. 6(b)]. Also presented in the two figures is the evolution of the local surface tension at the neck σ_{neck} with time from breakup, as surmised by Roché *et al.* ($\gamma \equiv \sigma_{\text{neck}}$) in Fig. 6(a) and obtained directly from our simulations in Fig. 6(b). First, these figures make plain that the slopes of the curves that depict how $R_{\min}$ scales with negative time from breakup obtained from experiments are in excellent agreement with those obtained from simulations, a finding that is a testimony to the high quality of the high-speed imaging experiments reported in Ref. [14]. By contrast, the values of σ_{neck} surmised by Roché *et al.* [14] deviate significantly from the actual values predicted from the simulations, thereby casting doubt on their assumption that σ_{neck} alone governs the thinning rate. The results presented in Fig. 6 therefore provide further proof that Marangoni stress contributions cannot be neglected in the pinch-off of surfactant-laden liquid threads, and that any theories or predictions in the literature that claim otherwise are hence inherently unphysical and likely incorrect.

V. CONCLUDING REMARKS AND OUTLOOK

In this paper, we have resolved the controversy as to whether surface tension lowering or surface tension gradients (Marangoni stresses) is responsible for reduced rates of thinning and microthread cascades during breakup of surfactant-covered drops and/or jets. Surfactant adsorption onto interfaces

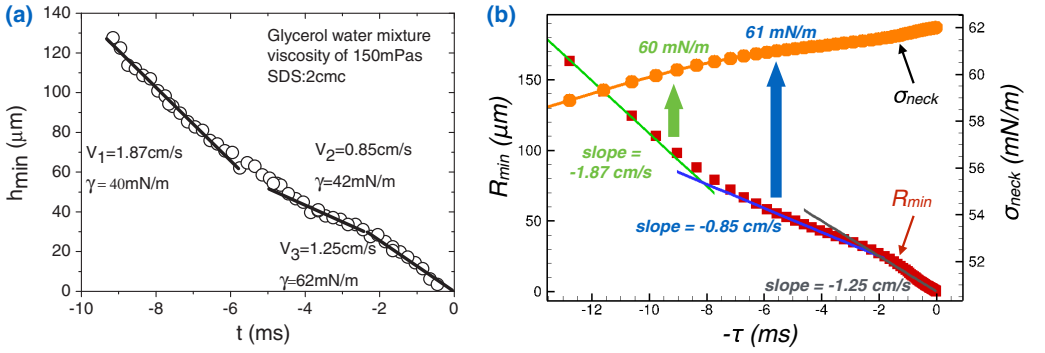

FIG. 6. Direct comparisons of simulations with experimental results and local surface tension predictions from Roché *et al.* [14]. (a) Figure 4(b) from Roché *et al.* [14] showing scaling of the minimum neck radius ($h_{\min} \equiv R_{\min}$) with negative time from breakup ($t \equiv -\tau$) along with predictions of the local surface tension at the neck ($\gamma \equiv \sigma_{\text{neck}}$). The values of the slopes of the radial scaling result in three distinct regimes, reported as V_1 through V_3. (b) Simulation results for the same values of the dimensionless parameters as in (a). Here, Oh $= 0.667$, $\Gamma_0 = 0.56$, $\beta = 0.4$, and Pe $= 1\,000$ (see the Appendix). Excellent agreement between experiments and simulations is observed in the $R_{\min}$ versus $-\tau$ scaling results. The σ_{neck} values that are directly extracted from the simulations, however, deviate significantly from the estimates from the experiments. In the simulations, the surface tension at the neck rises steadily and tends toward its value at the interface between a pure fluid and air, as would be expected due to continuous evacuation of surfactants from the neck as pinch-off is approached.

and the accompanying surface tension lowering and gradients arise in myriad free-surface flows involving drop breakup and coalescence and thin films, among others (see below). In many situations, it would be inordinately difficult to ascertain experimentally which of these two mechanisms dominates. We show that in simulations, however, Marangoni stresses can be turned off while retaining surfactant-induced lowering of surface tension, thereby unequivocally determining as to which of the two effects is the dominant mechanism by which surfactants affect any free-surface flow.

Although it was demonstrated by computation alone in Ref. [9] that microthread cascades can occur in the presence of surfactants, a definitive explanation as to the cause of these cascades and a number of other significant insights into the pinch-off of surfactant-covered threads were lacking in Ref. [9] but are presented in this paper. Specifically, the following list summarizes the significant accomplishments of the present work over Ref. [9] and makes clear that the present paper is much broader in scope and hence tantamount to a major advance over Ref. [9] rather than being simply an extension of it.

(a) In contrast to Ref. [9], it is demonstrated here that the Marangoni stress is the dominant mechanism by which surfactants affect pinch-off of liquid threads. This is a significant finding because, as stated in the Introduction, a number of recent works on the subject had made the assumption that is contrary to this fact.

(b) Whereas Ref. [9] presents purely computational results, we show the occurrence of microthread cascades in pinch-off of surfactant-laden liquid threads in laboratory experiments.

(c) Also in contrast to Ref. [9], we elucidate the mechanism by which Marangoni and viscocapillary stresses conspire to give rise to the cascades.

(d) Here, we show a direct comparison between scaling results obtained from experiments and simulations that verifies the existence of the heretofore unknown intermediate VWM scaling regime. At the time Ref. [9] was published, this regime was unknown [43] and, furthermore, the existence of such intermediate scaling regimes during pinch-off of even surfactant-free threads had not yet been discovered [41,42].

(e) In this paper, it has also been shown how numerical simulations can be used as investigative tools to selectively observe the effects of a physical mechanism (Marangoni stress) in isolation of others, a feat that would be virtually impossible to accomplish experimentally.

Our approach can be applied to other surfactant-laden free-surface flows where the role of Marangoni stresses have heretofore remained unclear. One example is tip streaming from drops subjected to extensional flows [45], a process that is greatly enhanced by surfactants [46] and is key to the dispersant action of surfactants in emulsification [47] and enhanced oil recovery [48]. Theoretical treatments on this subject [49,50] have not clarified whether local surface tension lowering or Marangoni stress primarily drives these processes. A similar debate exists in dip coating of surfactant solutions—the classical Landau-Levich problem—where surfactants lead to thicker films [51,52] and stagnation zone motion is important [53]. Similarly, our approach can be used to shed light on observations that have arisen in studies of sessile drop evaporation [54], where drops of whiskey are known to preclude coffee rings and instead to yield uniform stains—a feature that is desired in the coatings industry. While surfactants are known to alter drop evaporation stains [55] and the presence of naturally occurring phospholipid surfactants in whiskey is being considered as the probable cause of unusual stains, whether the observed phenomena can be attributed primarily to the action of Marangoni stresses in the whiskey stain example and many other free-surface flows remain open problems in science.

When studying experimentally the effects of surfactants on dynamics of pinch-off, researchers have found it convenient typically to rely on either the breakup of stretching liquid bridges [13,16,22] or dripping or jetting from nozzles [14,15,56]. Recently, Sharma and collaborators [57] developed a new technique of dripping onto a substrate to study the thinning dynamics of polymeric liquid bridges. Adoption of this setup to examine the dynamics of surfactant-laden liquids can provide an exciting new approach for studying the dynamics of thread pinch-off in the presence of surfactants.

Another important area where the results of, and the approach used, in this paper can make an impact is in studying breakup of free-surface flows where surface rheological effects play a role. It has recently been shown how accurate measurement of surface viscosities is not only challenging but made virtually impossible by the complex interactions between stresses due to surface viscosities and Marangoni stresses when a mixed flow is generated by a probe [58]. Thus, unreliable and inconsistent values of surface viscosities persist in the literature and have hindered the clarification of the true role of surface rheology in many free-surface flows including ones exhibiting breakup and finite-time singularities. Therefore, the approach adopted in this paper may be utilized to advantage to filter out the effects of Marangoni stress from experimental data so that the effects of surface viscosities can be inferred with greater precision than before. Indeed, it has recently been suggested that surface rheology could affect capillary thinning and pinch-off at small scales [59,60]. Accurate and realistic measurements of surface viscosities would be essential in order to verify the claims made in these aforementioned publications and to extend their implications to other free-surface flows involving breakup.

ACKNOWLEDGMENT

We thank Bausch and Lomb and the Gedge Professorship to O.A.B. for support.

APPENDIX: COMPARING SIMULATIONS AND EXPERIMENTS

In order to compare scaling results obtained from simulations, in which the surfactant is insoluble in the bulk liquid and confined to the interface, and those from experiments, in which the surfactant is soluble in the bulk liquid, as shown in Figs. 4(e) and 4(f) and Fig. 6, it is essential to match the values of the dimensionless groups used in the simulations with ones extracted from the reported or measured experimental parameters. Since the process used in both figures is identical, we provide here the details of the process for the comparison study carried out with the experiments of Roché *et al.* [14] shown in Fig. 6.

Roché *et al.* use a nozzle of diameter of 2 mm, i.e., $R = 1$ mm, report that the glycerol-water mixture used as the drop liquid had a viscosity of $\mu = 150$ mPa s and density of $\rho = 815.21$ kg m^{-3}, and further report that the surface tension of the interface between the pure liquid and air obtained from tensiometry was $\tilde{\sigma}_p = 62$ mN m^{-1}. From these values of the experimental parameters, the Ohnesorge number to be used in the simulations is then given by

$$\mathrm{Oh} = \frac{\mu}{\sqrt{\rho R \sigma_p}} = 0.667. \tag{A1}$$

The next important piece of information is the maximum packing concentration Γ_m of SDS at the air-water interface, which is reported by Chang and Franses [61] to be about 1×10^{-5} mol m^{-2}. One can then calculate the dimensionless surfactant strength parameter β at room temperature ($T = 298$ K) to be

$$\beta = \frac{\Gamma_m R_g T}{\sigma_p} \approx 0.4. \tag{A2}$$

The liquid in Roché *et al.*'s experiments is loaded with SDS at a bulk concentration of 2 cmc. The initial condition of surfactant concentration in the simulations, on the other hand, is described by the initial (dimensionless) surface concentration Γ_0 which equals $\tilde{\Gamma}_0/\Gamma_m$. In the experiments, while the total surfactant loading exceeds the cmc, the monomer concentration remains equal to the value at the cmc value as the excess surfactant molecules aggregate in micellar forms [19]. Therefore, the appropriate value of the surface concentration of SDS at the start of the experiment, $\tilde{\Gamma}_0$, equals the surface concentration at equilibrium with the 1 cmc bulk concentration. This value can be obtained directly from the surface tension measurements. Roché *et al.* [14] report the surface tension of the SDS-loaded system at a bulk concentration of 2 cmc is $\tilde{\sigma}_0 = 40$ mN m^{-1}. The dimensionless initial surface tension is therefore $\sigma_0 = \tilde{\sigma}_0/\sigma_p = 0.67$. Armed with this information, the initial dimensionless surface concentration can be extracted by using the Szyszkowski equation of state as

$$\Gamma_0 = 1 - \exp\left(\frac{\sigma_0 - 1}{\beta}\right) = 0.56. \tag{A3}$$

Thus, the initial value of the surface concentration is well below the maximum packing concentration, thereby justifying that the equation of state can be safely used even when the bulk concentration of surfactant is above the cmc.

The last dimensionless group to be extracted from the experimental parameters is the surface Péclet number Pe. The value of this dimensionless group is not readily available from the reported experimental data. However, it is well known that when $\mathrm{Pe} \gg 1$, the relative importance of diffusive transport is negligible compared to convective transport and the dynamical response during capillary thinning asymptotes to that of a thread exhibiting purely convective transport when $\mathrm{Pe} \geqslant O(10)$ [10]. As typical values of Pe for aqueous surfactant systems lie in the range 10^2–10^6 [22], we take the value of $\mathrm{Pe} = 1\,000$ in all of our simulations. Reassuringly, simulations carried out by varying Pe between 10^2 and 10^4, with all other dimensionless parameters kept the same, yielded identical results.

Repeating this procedure for a 70 wt % glycerol-water mixture that is loaded once again with SDS at a bulk concentration of 2 cmc and that is dripping from a tube of radius of $R = 1.57$ mm, it can be easily shown that $\mathrm{Oh} = 0.07$, $\beta \approx 0.4$, and $\Gamma_0 = 0.6$, as in Figs. 4(e) and 4(f).

The ultimate validation of the choice of values of the dimensionless parameters used in the simulations is provided by the excellent reproduction of the radial scaling results obtained from the experiments as shown in both Figs. 4(e) and 4(f) and Fig. 6. It should be emphasized that as explained in Sec. III, the solubility of SDS does not influence the surface concentration and its gradients along the interface because the surface adsorption of SDS, which has a time scale of the order of 100 ms, is significantly slower than the flow dynamics in the experiments which occur over the inertial-capillary, inertial-viscous, or viscous time scales which are all of the order of a few milliseconds.

[1] O. A. Basaran, Small-scale free surface flows with breakup: Drop formation and emerging applications, AIChE J. **48**, 1842 (2002).
[2] J. Eggers, Drop formation: An overview, Z. Angew. Math. Mech. **85**, 400 (2005).
[3] J. Eggers, Universal Pinching of 3D Axisymmetric Free-Surface Flow, Phys. Rev. Lett. **71**, 3458 (1993).
[4] J. Eggers and E. Villermaux, Physics of liquid jets, Rep. Prog. Phys. **71**, 1 (2008).
[5] X. D. Shi, M. P. Brenner, and S. R. Nagel, A cascade of structure in a drop falling from a faucet, Science **265**, 219 (1994).
[6] P. K. Notz and O. A. Basaran, Dynamics and breakup of a contracting liquid filament, J. Fluid Mech. **512**, 223 (2004).
[7] B. Derby, Inkjet printing of functional and structural materials: Fluid property requirements, feature stability, and resolution, Annu. Rev. Mater. Res. **40**, 395 (2010).
[8] O. A. Basaran, H. Gao, and P. P. Bhat, Nonstandard inkjets, Annu. Rev. Fluid Mech. **45**, 85 (2013).
[9] P. T. McGough and O. A. Basaran, Repeated Formation of Fluid Threads in Breakup of a Surfactant-Covered Jet, Phys. Rev. Lett. **96**, 054502 (2006).
[10] B. Ambravaneswaran and O. A. Basaran, Effects of insoluble surfactants on the nonlinear deformation and breakup of stretching liquid bridges, Phys. Fluids **11**, 997 (1999).
[11] M.-L. E. Timmermans and J. R. Lister, The effect of surfactant on the stability of a liquid thread, J. Fluid Mech. **459**, 289 (2002).
[12] R. V. Craster, O. K. Matar, and D. T. Papageorgiou, Pinchoff and satellite formation in surfactant covered viscous threads, Phys. Fluids **14**, 1364 (2002).
[13] Y.-C. Liao, H. J. Subramani, E. I. Franses, and O. A. Basaran, Effects of soluble surfactants on the deformation and breakup of stretching liquid bridges, Langmuir **20**, 9926 (2004).
[14] M. Roché, M. Aytouna, D. Bonn, and H. Kellay, Effect of Surface Tension Variations on the Pinch-Off Behavior of Small Fluid Drops in the Presence of Surfactants, Phys. Rev. Lett. **103**, 264501 (2009).
[15] M. Robert De Saint Vincent, J. Petit, M. Aytouna, J. P. Delville, D. Bonn, and H. Kellay, Dynamic interfacial tension effects in the rupture of liquid necks, J. Fluid Mech. **692**, 499 (2012).
[16] N. M. Kovalchuk, E. Nowak, and M. J. H. Simmons, Effect of soluble surfactants on the kinetics of thinning of liquid bridges during drops formation and on size of satellite droplets, Langmuir **32**, 5069 (2016).
[17] V. G. Levich and V. S. Krylov, Surface-tension-driven phenomena, Annu. Rev. Fluid Mech. **1**, 293 (1969).
[18] L. E. Scriven and C. V. Sternling, The Marangoni effects, Nature (London) **187**, 186 (1960).
[19] J. C. Berg, *An Introduction to Interfaces & Colloids: The Bridge to Nanoscience* (World Scientific, Singapore, 2010).
[20] J. Plateau, Recherches expérimentales et théorique sur les figures d'équilibre d'une masse liquide sans pesanteur, Acad. Sci. Bruxelles Mém. **XXIII**, 5 (1849).
[21] Lord Rayleigh, On the instability of jets, Proc. London Math. Soc. **10**, 4 (1879).
[22] Y.-C. Liao, E. I. Franses, and O. A. Basaran, Deformation and breakup of a stretching liquid bridge covered with an insoluble surfactant monolayer, Phys. Fluids **18**, 022101 (2006).
[23] O. A. Basaran and F. K. Wohlhuter, Effect of nonlinear polarization on shapes and stability of pendant and sessile drops in an electric (magnetic) field, J. Fluid Mech. **244**, 1 (1992).
[24] J. Q. Feng and O. A. Basaran, Shear-flow over a translationally symmetrical cylindrical bubble pinned on a slot in a plane wall, J. Fluid Mech. **275**, 351 (1994).
[25] T. W. Patzek, R. E. Benner, Jr., O. A. Basaran, and L. E. Scriven, Nonlinear oscillations of inviscid free drops, J. Comput. Phys. **97**, 489 (1991).
[26] E. D. Wilkes, S. D. Phillips, and O. A. Basaran, Computational and experimental analysis of dynamics of drop formation, Phys. Fluids **11**, 3577 (1999).
[27] K. N. Christodoulou and L. E. Scriven, Discretization of free surface flows and other moving boundary problems, J. Comput. Phys. **99**, 39 (1992).
[28] R. Suryo and O. A. Basaran, Local dynamics during pinch-off of liquid threads of power law fluids: Scaling analysis and self-similarity, J. Non-Newtonian Fluid Mech. **138**, 134 (2006).
[29] P. P. Bhat, O. A. Basaran, and M. Pasquali, Dynamics of viscoelastic liquid filaments: Low capillary number flows, J. Non-Newtonian Fluid Mech. **150**, 211 (2008).

[30] R. T. Collins, K. Sambath, M. T. Harris, and O. A. Basaran, Universal scaling laws for the disintegration of electrified drops, Proc. Natl. Acad. Sci. USA **110**, 4905 (2013).
[31] C. R. Anthony, P. M. Kamat, S. S. Thete, J. P. Munro, J. R. Lister, M. T. Harris, and O. A. Basaran, Scaling laws and dynamics of bubble coalescence, Phys. Rev. Fluids **2**, 083601 (2017).
[32] V. Garg, P. M. Kamat, C. R. Anthony, S. S. Thete, and O. A. Basaran, Self-similar rupture of thin films of power-law fluids on a substrate, J. Fluid Mech. **826**, 455 (2017).
[33] O. A. Basaran, Nonlinear oscillations of viscous liquid drops, J. Fluid Mech. **241**, 169 (1992).
[34] P. M. Gresho and R. L. Sani, *Incompressible Flow and the Finite Element Method, Volume 1: Advection-Diffusion and Isothermal Laminar Flow* (John Wiley and Sons, New York, 2000).
[35] G. Strang and G. Fix, *An Analysis of the Finite Element Method* (Prentice-Hall, Englewood Cliffs, NJ, 1973).
[36] P. Hood, Frontal solution program for unsymmetric matrices, Int. J. Numer. Methods Eng. **10**, 379 (1976).
[37] Y. J. Chen and P. H. Steen, Dynamics of inviscid capillary breakup: Collapse and pinchoff of a film bridge, J. Fluid Mech. **341**, 245 (1997).
[38] R. F. Day, E. J. Hinch, and J. R. Lister, Self-Similar Capillary Pinchoff of an Inviscid Fluid, Phys. Rev. Lett. **80**, 704 (1998).
[39] N. Ashgriz and F. Mashayek, Temporal analysis of capillary jet breakup, J. Fluid Mech. **291**, 163 (1995).
[40] P. K. Notz, A. U. Chen, and O. A. Basaran, Satellite drops: Unexpected dynamics and change of scaling during pinch-off, Phys. Fluids **13**, 549 (2001).
[41] J. R. Castrejón-Pita, A. A. Castrejón-Pita, S. S. Thete, K. Sambath, I. M. Hutchings, E. J. Hinch, J. R. Lister, and O. A. Basaran, Plethora of transitions during breakup of liquid filaments, Proc. Natl. Acad. Sci. USA **112**, 4582 (2015).
[42] Y. Li and J. E. Sprittles, Capillary breakup of a liquid bridge: Identifying regimes and transitions, J. Fluid Mech. **797**, 29 (2016).
[43] Q. Xu, Y.-C. Liao, and O. A. Basaran, Can Surfactant Be Present at Pinch-Off of a Liquid Filament? Phys. Rev. Lett. **98**, 054503 (2007).
[44] D. T. Papageorgiou, On the breakup of viscous liquid threads, Phys. Fluids **7**, 1529 (1995).
[45] R. Suryo and O. A. Basaran, Tip streaming from a liquid drop forming from a tube in a co-flowing outer fluid, Phys. Fluids **18**, 082102 (2006).
[46] C. D. Eggleton, T.-M. Tsai, and K. J. Stebe, Tip Streaming from a Drop in the Presence of Surfactants, Phys. Rev. Lett. **87**, 048302 (2001).
[47] T. Ward, M. Faivre, and H. A. Stone, Drop production and tip-streaming phenomenon in a microfluidic flow-focusing device via an interfacial chemical reaction, Langmuir **26**, 9233 (2010).
[48] B. Gopalan and J. Katz, Turbulent Shearing of Crude Oil Mixed with Dispersants Generates Long Microthreads and Microdroplets, Phys. Rev. Lett. **104**, 054501 (2010).
[49] Y.-H. Tseng and A. Prosperetti, Local interfacial stability near a zero vorticity point, J. Fluid Mech. **776**, 5 (2015).
[50] R. Krechetnikov, Structure of Marangoni-driven singularities, Phys. Fluids **24**, 022111 (2012).
[51] O. Ou Ramdane and D. Quéré, Thickening factor in Marangoni coating, Langmuir **13**, 2911 (1997).
[52] R. Krechetnikov and G. M. Homsy, Surfactant effects in the Landau-Levich problem, J. Fluid Mech. **559**, 429 (2006).
[53] E. Ramé, The stagnation point in Marangoni-thickened Landau-Levich type flows, Phys. Fluids **19**, 17 (2007).
[54] B. Verberck, Fluid dynamics: Spirited away, Nat. Phys. **12**, 291 (2016).
[55] T. Still, P. J. Yunker, and A. G. Yodh, Surfactant-induced Marangoni eddies alter the coffee-rings of evaporating colloidal drops, Langmuir **28**, 4984 (2012).
[56] X. G. Zhang and O. A. Basaran, An experimental study of dynamics of drop formation, Phys. Fluids **7**, 1184 (1995).
[57] J. Dinic, Y. Zhang, L. N. Jimenez, and V. Sharma, Extensional relaxation times of dilute, aqueous polymer solutions, ACS Macro Lett. **4**, 804 (2015).
[58] G. J. Elfring, L. G. Leal, and T. M. Squires, Surface viscosity and Marangoni stresses at surfactant laden interfaces, J. Fluid Mech. **792**, 712 (2016).

[59] A. Ponce-Torres, M. A. Herrada, J. M. Montanero, and J. M. Vega, Linear and nonlinear dynamics of an insoluble surfactant-laden liquid bridge, Phys. Fluids **28**, 112103 (2016).

[60] A. Ponce-Torres, J. M. Montanero, M. A. Herrada, E. J. Vega, and J. M. Vega, Influence of the Surface Viscosity on the Breakup of a Surfactant-Laden Drop, Phys. Rev. Lett. **118**, 024501 (2017).

[61] C.-H. Chang and E. I. Franses, Adsorption dynamics of surfactants at the air/water interface: A critical review of mathematical models, data, and mechanisms, Colloids Surf. A **100**, 1 (1995).